Analysis and design of long-period waveguide-grating couplers

Bai, Yukun; Chiang, Kin Seng

Published in:
Journal of Lightwave Technology

Published: 01/12/2005

Document Version:
Post-print, also known as Accepted Author Manuscript, Peer-reviewed or Author Final version

Published version (DOI):
10.1109/JLT.2005.858253

Publication details:
Bai, Y., & Chiang, K. S. (2005). Analysis and design of long-period waveguide-grating couplers. *Journal of Lightwave Technology*, *23*(12), 4363-4373. https://doi.org/10.1109/JLT.2005.858253

Bai, Y., & Chiang, K. S. (2005). Analysis and design of long-period waveguide-grating couplers. Journal of Lightwave Technology, 23(12), 4363-4373. https://doi.org/10.1109/JLT.2005.858253.

Analysis and Design of Long-Period Waveguide Grating Couplers

Yukun Bai and Kin Seng Chiang, *Member, IEEE, Fellow, OSA*

Optoelectronics Research Centre and Department of Electronic Engineering,

City University of Hong Kong, Hong Kong, China

* Tel: 852-27889605; Fax: 852-27887791; Email: eeksc@cityu.edu.hk

Abstract — By means of the coupled-mode theory, we analyze an optical waveguide coupler consisting of two parallel identical waveguides, each of which contains a uniform long-period grating. We show that light can be coupled effectively between the two waveguides through the gratings at specific wavelengths (the resonance wavelengths) in the absence of evanescent-field coupling. The conditions for achieving 100 % coupling efficiency at the resonance wavelength under various situations are highlighted and the effects of the grating parameters on the transmission spectra of the coupler are illustrated with examples. We also present practical waveguide designs for the realization of the coupler. Long-period waveguide grating coupler is a versatile waveguide structure and should find potential applications in optical filtering, add/drop multiplexing, and optical switching.

Index Terms — Coupled-mode theory, long-period gratings, optical couplers, optical filters, optical waveguides.

I. INTRODUCTION

A long-period fiber grating (LPFG), which is normally formed by introducing a periodic modulation of the refractive index along the core of a single-mode fiber with a pitch of the order of 100 μm, allows effective light coupling between the guided mode and the cladding modes of the fiber and thus results in a transmission spectrum consisting of a series of rejection bands centered at specific wavelengths (the resonance wavelengths) [1]. LPFGs have been developed into many useful devices, including band-rejection filters [1],[2], gain flatteners for erbium-doped fiber amplifiers [3]-[5], dispersion compensators [6], and various kinds of sensors [7]-[10]. In most applications with such devices, the light energy coupled to the cladding mode is either absorbed or made to radiate away. This restricts an LPFG to function as no more than a band-rejection filter. Recently, add/drop multiplexers in the form of two coupled parallel LPFGs have been demonstrated [11]-[14]. The outputs from the two gratings are complementary to each other, one showing band-rejection characteristics and the other showing band-pass characteristics. The structure of two parallel LPFGs thus offers additional flexibility in producing new functions. In practice, however, maintaining two fibers in strict parallel for the provision of stable and efficient add/drop operation is very much a challenge in packaging. On the other hand, the packaging problem can be eased if the device is formed in planar waveguides on the same substrate. The availability of a wide variety of waveguide geometries and materials also offers much flexibility in the design of compact and robust devices, particularly, tunable devices [15],[16]. As a matter of fact, widely tunable long-period waveguide gratings (LPWGs) in glass and polymer waveguides have been demonstrated [17]-[19]. Thermally induced long-period gratings in polymer waveguides have also been reported recently [20],[21].

In this paper, we study theoretically a waveguide coupler that consists of two parallel uniform long-period gratings. The light-coupling behavior in such an LPWG coupler is different from that in an LPFG coupler. In an LPFG coupler, light is coupled between the guided mode and the cladding mode of the individual fiber

through the individual grating and the cladding modes of the two parallel fibers are coupled by evanescent-field coupling [14]. It is the evanescent-field coupling between the cladding modes of the two fibers that makes possible the transfer of light from one fiber to the other. In an LPWG coupler, because the waveguide cores are embedded in the same cladding, light is coupled to the cladding mode of the entire structure from the guided mode through the grating in the launching waveguide and, at the same time, light is coupled from the same cladding mode to the guided mode of the neighboring waveguide through the other grating. The process involves only a cladding mode of the composite structure and, therefore, no evanescent-field coupling between cladding modes is present. As in a conventional directional coupler, there may exist evanescent-field coupling between the guided modes of the two waveguide cores, but such coupling can be made negligible by placing the two cores sufficiently far apart from each other. In other words, unlike an LPFG coupler, an LPWG coupler does not rely on any evanescent-field coupling and thus results in a more compact device with a good tolerance in the core separation. In the first part of the study, we use the coupled-mode theory to analyze the transmission spectra of the coupler and highlight the conditions for achieving 100 % coupling efficiency. An offset between the two parallel gratings along the direction of wave propagation is allowed. In the second part of the study, we present some practical waveguide designs to show that LPWG couplers can be realized readily with conventional waveguide structures.

II. COUPLED-MODE ANALYSIS

An LPWG coupler is shown schematically in Fig. 1. The coupler consists of two parallel identical rectangular single-mode cores, which are separated by a distance d and embedded in a rectangular cladding with thickness t and width s. Each of the cores contains a corrugated grating with length L, corrugation depth Δh, and pitch Λ. As shown in Fig. 1, the two gratings may be displaced in the light propagation direction z by a distance, denoted as z_1. The interaction region of the coupler is then divided into three sections: Section I, Section II, and Section III. While corrugated gratings are assumed in Fig. 1, it should be understood that our theory applies equally

well to phase gratings and the gratings need not be located in the cores (they can be located in the cladding [22]). Here we assume that the two cores are sufficiently far apart and the grating is so weak that it can be treated as a perturbation to the original waveguide structure. Therefore, the mode coupling between the two cores can be described by the conventional coupled-mode theory [23],[24]. The pitch of the grating is so chosen that light is coupled between the guided mode of the individual core to a cladding mode of the entire composite structure. According to the phase-matching condition [1], the resonance wavelength λ_0, namely, the wavelength at which the mode coupling is most effective, is given by

$$\lambda_0 = (N_{\mathrm{co}} - N_{\mathrm{cl}})\Lambda, \tag{1}$$

where N_{co} and N_{cl} are the effective indices of the guided mode of the individual core and the cladding mode of the entire structure, respectively.

In practice, light is launched into only one of the cores (the launching core) and collected from both cores (the launching core and the tapping core). There are three coupling processes involved: (i) coupling between the guided mode of the launching core and the cladding mode of the entire structure, (ii) coupling between the cladding mode of the entire structure and the guided mode of the tapping core, and (iii) evanescent-field coupling between the two cores. We denote the amplitudes of the guided modes of the launching and tapping cores as $A(z)$ and $\bar{A}(z)$, respectively, and that of the cladding mode as $B(z)$. In Section II of the coupler, where both gratings are present in the z direction, all three processes are involved and the coupled-mode equations are given by

$$\frac{dA}{dz} = -j\kappa B\exp(j\delta z) - jC\bar{A}, \tag{2}$$

$$\frac{dB}{dz} = -j\kappa A\exp(-j\delta z) \mp j\kappa\bar{A}\exp(-j\delta z), \tag{3}$$

$$\frac{d\bar{A}}{dz} = \mp j\kappa B\exp(j\delta z) - jCA, \tag{4}$$

where $\delta = (2\pi/\Lambda)(\lambda_0/\lambda - 1)$ is the phase-detuning parameter that measures the deviation of the free-space operation wavelength λ from λ_0, κ is the coupling coefficient of the gratings, and C is the evanescent-field coupling coefficient between the two cores. As the coupler has a symmetrical geometry, the cladding mode of the coupler has either a symmetrical or an anti-symmetrical field distribution with respect to the y axis. The negative and positive signs in Eqs. (3) and (4) apply to the symmetrical and anti-symmetrical cladding modes, respectively. In Section I of the coupler, where only Processes (i) and (iii) are present, the coupled-mode equations are simplified to

$$\frac{dA}{dz} = -j\kappa B\exp(j\delta z) - jC\overline{A}, \tag{5}$$

$$\frac{dB}{dz} = -j\kappa A\exp(-j\delta z), \tag{6}$$

$$\frac{d\overline{A}}{dz} = -jCA. \tag{7}$$

Similarly, in Section III of the coupler, where only Processes (ii) and (iii) are present, the coupled-mode equations are given by

$$\frac{dA}{dz} = -jC\overline{A}, \tag{8}$$

$$\frac{dB}{dz} = \mp j\kappa\overline{A}\exp(-j\delta z), \tag{9}$$

$$\frac{d\overline{A}}{dz} = \mp j\kappa B\exp(j\delta z) - jCA. \tag{10}$$

The coupling efficiency of the coupler can be defined as the fractional power coupled to the tapping core when light is launched only into the launching core, namely,

$$\eta = \frac{\left|\overline{A}(z_3)\right|^2}{\left|A(0)\right|^2}, \tag{11}$$

with $\overline{A}(0) = B(0) = 0$. By following the method in [14], these coupled-mode equations can be solved analytically and the solutions are given in Appendix.

III. TRANSMISSION CHARACTERISTICS

In this section, the transmission characteristics of the LPWG coupler are analyzed with examples. The conditions for achieving 100 % coupling efficiency at the resonance wavelength are discussed. Throughout the study, light is assumed to be launched into only one of the cores, i.e., $A(0)=1$ and $B(0)=\overline{A}(0)=0$. Three different cases are discussed, according to the offset distance between the two gratings.

A. Offset $z_1 = 0$

In this case, the two gratings are perfectly aligned to each other and the coupling processes are described by Eqs. (2)-(4). The analytical solutions are given in Section A of Appendix. We consider only the case that light in the core is coupled to the symmetrical cladding mode. As shown in Appendix, the transmission spectra for coupling to the anti-symmetrical cladding mode are just the mirror images of those for coupling to the symmetrical cladding modes with respect to the resonance wavelength (so the transmission spectra for the symmetrical and anti-symmetrical cladding modes are identical if the spectra are symmetrical with respect to the resonance wavelength). The conditions for achieving 100% coupling efficiency at the resonance wavelength (i.e., $\delta = 0$) are found as

$$CL = \frac{2}{3} p\pi , \tag{12}$$

$$\kappa L = \frac{\pi}{\sqrt{2}} \left[q^2 - \left(\frac{p}{3} \right)^2 \right]^{\frac{1}{2}}, \tag{13}$$

where L is the length of the gratings. In these equations, when p is an even integer (0, 2, 4, …), q is an odd integer (1, 3, 5, …), whereas when p is an odd integer (1, 3, 5, …), q is an even integer (2, 4, 6, …). In any case, $p < 3q$ must be satisfied.

In practice, it is simpler to design a coupler without the influence of evanescent-field coupling between the two cores (i.e., $C = 0$). This can be done by using a sufficiently large core separation. The power transfer between the two cores is then achieved solely by the gratings. Putting $p = 0$ in Eqs. (12) and (13) (i.e.,

assuming $C = 0$), we obtain from Eq. (13)

$$\kappa L = \frac{(2n+1)\pi}{\sqrt{2}}, \qquad n = 0, 1, 2, \ldots. \tag{14}$$

which is a simple formula for the design of an efficient LPWG coupler. The transmission spectra for $\kappa L = \pi/\sqrt{2}$ ($n = 0$), $3\pi/\sqrt{2}$ ($n = 1$), and $5\pi/\sqrt{2}$ ($n = 2$) are shown in Fig. 2(a), Fig. 3(a), and Fig. 4(a), respectively, while the corresponding coupling dynamics at the resonance wavelength ($\delta = 0$) are shown in Fig. 2(b), Fig. 3(b), and Fig. 4(b), respectively. It can be seen from Fig. 2(a) that, for $n = 0$, the transmission spectrum of the launching core shows a clean band-rejection characteristic while that of the tapping core shows a clean band-pass characteristic. The coupler thus functions as an add/drop multiplexer in the same way as an LPFG coupler [14]. However, for $n > 0$, there exist n wavelengths on both sides of the resonance wavelength, at which the coupling is significant and, in fact, can reach 100 %, as shown in Fig. 3(a) and Fig. 4(a). For each value of n, the values of δL that give 100 % coupling are solved as

$$\delta L = \pm 4\pi h \tag{15}$$

where h is an integer that satisfies

$$h = \sqrt{(m+n+1)(m-n)}, \qquad m\ (\geq n)\text{: a positive integer} \tag{16}$$

It is noted that $h = 0$ (corresponding to $m = n$) gives the resonance wavelength. In addition to the resonance wavelength, we find, for example, $h = 2$ with $m = 2$ for $n = 1$, and $h = 6$ with $m = 6$ for $n = 2$. The corresponding values of δL are $\pm 8\pi$ and $\pm 24\pi$, respectively, which are shown in the transmission spectra in Fig. 3(a) and Fig. 4(a), respectively. The coupling dynamics at $\delta L = 8\pi$ for $n = 1$ is shown in Fig. 3(c) and that at $\delta L = 24\pi$ for $n = 2$ is shown in Fig. 4(c). These dynamics are markedly different from those shown in Fig. 3(b) and Fig. 4(b) for $\delta L = 0$.

The 3-dB bandwidth of the rejection band centered at $\delta L = 0$, normalized with respect to $\lambda_0 \Lambda / L$, is shown in Fig. 5. It can be seen that the 3-dB bandwidth

approaches $\lambda_0\Lambda/L$ quickly as n increases, as confirmed by the derivation given in Section A of Appendix.

In the presence of evanescent-field coupling between the two cores, i.e., $C > 0$, 100 % coupling at the resonance wavelength is possible provided that Eqs. (12) and (13) are satisfied. As an example, we choose, according to Eqs. (12) and (13), $CL = 4\pi/3$ and $\kappa L = \pi/3\sqrt{5/2}$. The transmission spectra of the coupler and the coupling dynamics at the resonance wavelength are shown in Fig. 6(a) and Fig. 6(b), respectively. As shown in Fig. 6(a), while 100% coupling is achieved at the resonance wavelength, the transmission spectra are highly asymmetrical and significant coupling is also possible at other wavelengths. The effects of the coupling coefficient C on the transmission spectra of the coupler are shown in Fig. 7, where $\kappa L = \pi/\sqrt{2}$ is assumed. The effects of C are negligible when $CL < 0.01$, which can be regarded as a rule of thumb for the design of LPWG couplers.

B. Offset $0 < z_1 < L$

As in the case of an LPFG coupler, the transmission spectra of an LPWG coupler can be modified significantly by introducing an offset distance between the two gratings along the light propagation direction. Here we consider only the more practical situation where evanescent-field coupling between the two cores is negligible, i.e., $C = 0$. To analyze the effects of the offset, the coupled-mode equations for all the three sections shown in Fig. 1, i.e., Eqs. (2) – (10), are solved. The details of solving these equations are given in Appendix. The output amplitudes from one section are treated as the input amplitudes for the next section. We identify some special conditions where 100 % coupling at the resonance wavelength are guaranteed.

We set the offset distance z_1 to

$$z_1 = \frac{m\pi}{2\kappa}, \qquad m = 1, 2, 3, \ldots \tag{17}$$

which is the length required for coupling the light in the launching core to the cladding mode completely (m = 1, 3, …) or back to itself (m = 2, 4, …).The length of

the middle section can then be determined by Eq. (14), namely,

$$z_2 - z_1 = \frac{(2n+1)\pi}{\sqrt{2}\kappa}, \qquad n = 0, 1, 2, \ldots \tag{18}$$

The transmission spectra calculated for $m = 1$ and $n = 0$ are shown in Fig. 8(a) and the coupling dynamics at the resonance wavelength are shown in Fig. 8(b). Compared with Fig. 2(a), the transmission spectra shown in Fig. 8(a) contain more significant side lobes, which arise from the use of longer gratings. If an odd integer *m* is used in Eq. (17), i.e., the light in the launching core is coupled completely to the cladding mode at $z = z_1$, the length of the middle section can also be equal to

$$z_2 - z_1 = \frac{2n\pi}{\sqrt{2}\kappa}, \qquad n = 1, 2, 3, \ldots \tag{19}$$

so that the cladding mode is coupled back to itself. The cladding mode is finally coupled to the tapping core completely in the third section, which has the same length as the first section.

C. Offset $z_1 \geq L$

When the two gratings are displaced completely, i.e., $z_1 = L$, to achieve 100 % coupling, the light in the launching core must be coupled to the cladding mode completely at $z = z_1$. Therefore, the condition for 100% coupling at the resonance wavelength is simply given by

$$\kappa L = \left(n + \frac{1}{2}\right)\pi, \qquad n = 0, 1, 2, \ldots. \tag{20}$$

The transmission spectra calculated for $n = 0$ and the corresponding coupling dynamics at the resonance wavelength are shown in Fig. 9(a) and Fig. 9(b), respectively. Compared with the spectra shown in Fig. 8(a), the side lobes in this case are less significant. The transmission spectra of the coupler remain unchanged as the offset is increased further, i.e., $z_1 > L$.

IV. DESIGN EXAMPLES

In this section, we present design examples based on the waveguide structure shown in Fig. 1. The resonance wavelength λ_0 is around 1550 nm. The refractive indices of the core, the cladding, and the substrate are n_{core} = 1.537, n_{clad} = 1.505, and n_{sub} = 1.444, respectively. These values are typical of polymer films coated on silica [18]. The coupler is surrounded by air, i.e., n_{ex} = 1. The dimensions of the cores are fixed at $a = h$ = 3 μm, which ensure single-mode operation at 1550 nm. The cladding thickness t and the side width s are fixed at 4 μm and 6 μm, respectively. The composite waveguide structure is analyzed with a commercial full vector mode solver FIMMWAVE (Photon Design), which is based on the mode-matching method [25].

As discussed in the previous section, the two cores should be well separated to make the evanescent-field coupling coefficient C negligible. The coupling coefficient C is governed by the difference between the effective indices of the guided even (E_{11}) and odd (E_{21}) modes of the composite structure, N_e and N_o, which are solutions of the mode solver. To be specific, C is given by

$$C = \frac{N_e - N_o}{2} k_0 \tag{21}$$

where $k_0 = 2\pi/\lambda$ is the free-space wavenumber. The dependence of the effective indices N_e and N_o for both quasi-TE and quasi-TM polarizations on the core separation d is shown in Fig. 10. N_e and N_o are practically equal as the core separation is equal to 8 μm or larger. We therefore choose d = 8 μm for our design, in which case the E_{11} and E_{21} modes of the composite structure can be considered degenerate and the evanescent-field coupling between the two cores can be ignored.

The central task in the design of an LPWG is to determine the grating pitch Λ from the phase-matching condition Eq. (1). With C = 0, the effective index of the guided mode of the individual core is simply equal to the effective index of the E_{11} mode (or the E_{21} mode) of the composite structure (of the same polarization). There are, however, a large number of cladding modes supported by the composite structure (e.g., the E_{31}, E_{41}, E_{12}, E_{22}, … modes), which have different effective indices. In

principle, the LPWG can be designed to couple light from the E_{11} mode (the guided mode) to any of these cladding modes. According to Eq. (1), each coupled cladding mode provides a relation between the resonance wavelength λ_0 and the grating pitch Λ (the phase-matching curve). The phase-matching curves for four cladding modes of our structure are shown in Fig. 11(a), while the effective indices of the modes are shown in Fig. 11(b) as functions of the wavelength. The pitch of the LPWG can be determined readily from the curves in Fig. 11(a). Here we choose a pitch of 93.2 μm, which corresponds to the coupling to the E_{31} mode at a resonance wavelength of 1550 nm for the quasi-TE polarization. For this particular choice, the resonance wavelength is relatively polarization insensitive and the neighboring resonance wavelengths that result from couplings to other cladding modes are sufficiently far away from 1550 nm.

The coupling coefficient κ of the LPWG coupler is given by [16]

$$\kappa = \frac{k_0\left(n_{\text{core}}^2 - n_{\text{clad}}^2\right)}{\pi c \mu_0} \iint_S \vec{e}_A \cdot \vec{e}_B^{\,*} dS \tag{22}$$

where μ_0 and c are the permeability and the speed of light in vacuum, respectively, $\vec{e}_A$ and $\vec{e}_B$ are the normalized mode fields of the guided mode of the individual core and the cladding mode, respectively. The integration in Eq. (22) is performed over the area of the grating perturbation, which, for a corrugated grating, is the corrugated region [16] or, for a phase grating, the region of index modulation [15]. The dependence of the coupling coefficient κ on the corrugation depth Δh in the core (as defined in Fig. 1) is shown in Fig. 12 for the couplings to the E_{31} and E_{41} cladding modes at 1550 nm. The results for both quasi-TE and quasi-TM polarizations are given in the figure. For a typical grating length of 30 mm, the coupling coefficient κ required for 100 % coupling at λ_0 is 74 m^{-1}, which, according to Fig. 12, corresponds to a corrugation depth Δh of 221 nm for the coupling to the quasi-TE E_{31} cladding mode.

The transmission spectra for the coupling to the quasi-TE and quasi-TM E_{31}

cladding modes are shown in Fig. 13(a) and Fig. 13(b), respectively. Because the design is optimized for 100 % coupling at λ_0 for the quasi-TE polarization, the coupling efficiency for the quasi-TM polarization, though still high, is not 100 %. The resonance wavelengths for the two polarizations are also slightly different. The 3-dB bandwidths of the rejection bands are 6 nm at λ_0 = 1550 nm for the quasi-TE polarization and 4 nm at λ_0 = 1548 nm for the quasi-TM polarization.

V. CONCLUSION

We analyze in detail an LPWG coupler consisting of two parallel uniform long-period gratings with the coupled-mode theory. The conditions for achieving 100 % coupling efficiency at the resonance wavelength, whether the two gratings are perfectly aligned or displaced in the light propagation direction, are highlighted and discussed. For the generation of clean add/drop characteristics, it is necessary to design the coupler in such a way that the evanescent-field coupling between the two cores is negligible. The feasibility of designing an effective LPWG coupler is demonstrated with a specific example using a common waveguide structure. The issue of polarization dependence is also highlighted in the example. As in the case of a single LPWG [18], it should be possible to realize a polarization-insensitive LPWG coupler by designing the waveguide structure carefully. On the fabrication of the device, by using the direct UV-writing technique [26],[27], it should be possible to write an LPWG coupler while monitoring the growth of its transmission spectrum. In fact, direct UV writing has been proposed for the fabrication of grating-assisted couplers on glass waveguides [26]. Recently, LPWGs have been written in polymer waveguides with a 248-nm excimer laser [22]. The same technique should be applicable to the writing of polymer LPWG couplers. This real-time technique can relax substantially the tolerances in the grating parameters required for satisfying the 100 % coupling conditions. Passive LPWG couplers are expected to find applications as optical filters and broadband add/drop multiplexers. When thermo-optic or electro-optic tuning is incorporated into an LPWG coupler, as in the case of a single LPWG [17],[18],[21],[22], the coupler can function as a tunable add/drop filter or an optical switch.

ACKNOWLEDGEMENT

This work was supported by research grants from the Research Grants Council of the Hong Kong Special Administrative Region [Project No. CityU 1160/01E and CityU 1255/03E].

APPENDIX

A. Coupling of Three Modes

The general solutions to Eqs. (2)-(4) can be expressed in the following form:

$$A(z) = A(0)e^{j\gamma_A z} \tag{23a}$$

$$B(z) = B(0)e^{j\gamma_B z} \tag{23b}$$

$$\bar{A}(z) = \bar{A}(0)e^{j\bar{\gamma}_A z}. \tag{23c}$$

Putting the above equations into Eqs. (2)-(4) (assuming coupling to the symmetrical cladding mode) yields the following relations

$$\gamma_B = \gamma_A - \delta \tag{24a}$$

$$\bar{\gamma}_A = \gamma_A \tag{24b}$$

$$\left[\gamma_A^2 + (C-\delta)\gamma_A - (C\delta + 2\kappa^2)\right](\gamma_A - 1) = 0. \tag{24c}$$

The general solutions are then expressed as

$$A(z) = \sum_{n=1}^{3} A_n e^{j\gamma_{A_n} z} \tag{25a}$$

$$B(z) = \sum_{n=1}^{3} B_n e^{j\gamma_{B_n} z} \tag{25b}$$

$$\bar{A}(z) = \sum_{n=1}^{3} \bar{A}_n e^{j\bar{\gamma}_{A_n} z} \tag{25c}$$

where γ_{A_n} ($n = 1, 2, 3$) are the three roots of Eq. (24c) and the corresponding γ_{B_n} and $\bar{\gamma}_{A_n}$ are obtained from their relations with γ_{A_n} in Eqs. (24a) and (24b). Putting Eq. (25) into Eqs. (2)-(4), equalizing the coefficients of the same exponential terms on both sides of the equations, and applying the input conditions, we can find A_n, B_n

and $\overline{A}_n$ ($n = 1, 2, 3$) in terms of $A(0)$, $B(0)$ and $\overline{A}(0)$. Therefore, the mode amplitudes are finally obtained as

$$\begin{aligned} A(z) = \frac{1}{2Q}\left\{\left[Q\cos(Qz) - jS_2\sin(Qz)\right]e^{jS_1 z} + Qe^{jCz}\right\}A(0) \\ - j\frac{\kappa}{Q}\sin(Qz)e^{jS_1 z}\,B(0) \\ + \frac{1}{2Q}\left\{\left[Q\cos(Qz) - jS_2\sin(Qz)\right]e^{jS_1 z} - Qe^{jCz}\right\}\overline{A}(0) \end{aligned} \tag{26a}$$

$$\begin{aligned} B(z) = -j\frac{k}{Q}\sin(Qz)e^{-jS_2 z}A(0) \\ + \frac{1}{Q}e^{-jS_2 z}\left[jS_2\sin(Qz) + Q\cos(Qz)\right]B(0) \\ - j\frac{k}{Q}\sin(Qz)e^{-jS_2 z}\overline{A}(0) \end{aligned} \tag{26b}$$

$$\begin{aligned} \overline{A}(z) = \frac{1}{2Q}\left\{\left[Q\cos(Qz) - jS_2\sin(Qz)\right]e^{jS_1 z} - Qe^{jCz}\right\}A(0) \\ - j\frac{\kappa}{Q}\sin(Qz)e^{jS_1 z}\,B(0) \\ + \frac{1}{2Q}\left\{\left[Q\cos(Qz) - jS_2\sin(Qz)\right]e^{jS_1 z} + Qe^{jCz}\right\}\overline{A}(0) \end{aligned} \tag{26c}$$

where $S_1 = (\delta - C)/2$, $S_2 = (\delta + C)/2$ and $Q = \sqrt{S_2^2 + 2\kappa^2}$. For the input conditions $A(0) \neq 0$, $B(0) = \overline{A}(0) = 0$, the normalized modal powers are given by

$$|A(z)|^2 = \frac{1}{4}\left\{\left[\cos(Qz) + \cos(S_1 - C)z\right]^2 + \left[\frac{S_2}{Q}\sin(Qz) + \sin(S_1 - C)z\right]^2\right\}|A(0)|^2 \tag{27a}$$

$$|B(z)|^2 = \left[\frac{\kappa}{Q}\sin(Qz)\right]^2 |A(0)|^2 \tag{27b}$$

$$|\overline{A}(z)|^2 = \frac{1}{4}\left\{\left[\cos(Qz) - \cos(S_1 - C)z\right]^2 + \left[\frac{S_2}{Q}\sin(Qz) - \sin(S_1 - C)z\right]^2\right\}|A(0)|^2 \tag{27c}$$

where $S_1 = (\delta - C)/2$, $S_2 = (\delta + C)/2$ and $Q = \sqrt{S_2^2 + 2\kappa^2}$. Similar results are obtained for coupling to the anti-symmetrical cladding mode:

$$|A(z)|^2 = \frac{1}{4}\left\{\left[\cos(Qz)+\cos(S_1+C)z\right]^2+\left[\frac{S_2}{Q}\sin(Qz)-\sin(S_1+C)z\right]^2\right\}|A(0)|^2 \qquad (28a)$$

$$|B(z)|^2 = \left[\frac{\kappa}{Q}\sin(Qz)\right]^2|A(0)|^2 \qquad (28b)$$

$$|\bar{A}(z)|^2 = \frac{1}{4}\left\{\left[\cos(Qz)-\cos(S_1+C)z\right]^2+\left[\frac{S_2}{Q}\sin(Qz)+\sin(S_1+C)z\right]^2\right\}|A(0)|^2 \qquad (28c)$$

where $S_1=(\delta+C)/2$, $S_2=(C-\delta)/2$ and $Q=\sqrt{S_2^2+2\kappa^2}$. A comparison of (27a)-(27c) and (28a)-(28c) shows that the transmission spectra for coupling to the anti-symmetrical cladding mode are mirror images of their counterparts for coupling to the symmetrical cladding mode with respect to the resonance wavelength.

Putting $\delta=0$ into Eq. (27c) and setting $|\bar{A}(L)|^2=|A(0)|^2$, we obtain the conditions Eqs. (12) and (13) for 100 % coupling efficiency at the resonance wavelength. By substituting $C=0$ and $\kappa L=(2n+1)\pi/\sqrt{2}$ ($n=0, 1, 2, ...$) into Eq. (27c), we obtain Eq. (15) for the values of δL to give 100% coupling.

Substituting $C=0$ and $\kappa L=(2n+1)\pi/\sqrt{2}$ ($n=0, 1, 2, ...$) into Eq. (27c), and setting the normalized power to 1/2, we obtain an equation for δ_{3dB} , which is the value of δ at which 3-dB transmission is achieved. Under the condition $\kappa >> \delta_{3dB}$, we find

$$\cos(S_2L)=0 \qquad (29)$$

$$\delta_{3dB}=\frac{(2m+1)\pi}{L}, \qquad m=0, \pm1, \pm2, \ldots \qquad (30)$$

The corresponding wavelengths are

$$\lambda_m=\frac{\lambda_0}{1+\left(m+\frac{1}{2}\right)\frac{\Lambda}{L}}, \qquad m=0, \pm1, \pm2, \ldots \qquad (31)$$

For the two 3-dB wavelengths around the resonance wavelength, we set $m=-1$ and

$m = 0$ in Eq. (31) and find the 3-dB bandwidth $\Delta\lambda_{3\text{dB}} = \lambda_{-1} - \lambda_0$ as

$$\Delta\lambda_{3\text{dB}} = \frac{\lambda_0 \Lambda}{L}. \tag{32}$$

B. Coupling of Two modes

With $C = 0$, the solutions to Eqs. (5)-(7) are obtained as

$$A(z) = \frac{1}{Q} e^{jSz} \{ [Q\cos(Qz) - jS\sin(Qz)] A(0) - j\kappa \sin(Qz)\, B(0) \} \tag{33a}$$

$$B(z) = \frac{1}{Q} e^{-jSz} \{ - j\kappa \sin(Qz)\, A(0) + [jS\sin(Qz) + Q\cos(Qz)] B(0) \} \tag{33b}$$

where $S = \delta/2$ and $Q = \sqrt{S^2 + \kappa^2}$. Similar solutions can be written down for Eqs. (8)-(10).

REFERENCES

[1] A. M. Vengsarkar, P. J. Lemaire, J. B. Judkins, V. Bhatia, T. Erdogan, and J. E. Sipe, "Long-period fiber gratings as band-rejection filters," *J. Lightwave Technol*., vol. 14, pp. 58-65, 1996.

[2] X. J. Gu, "Wavelength-division multiplexing isolation fiber filter and light source using cascaded long-period fiber gratings," *Opt. Lett*., vol. 23, pp. 509-510, 1998.

[3] A. M. Vengsarkar, J. R. Pedrazzani, J. B. Judkins, P. J. Lemaire, N. S. Bergano, and C. R. Davidson, "Long-period fiber-grating-based gain equalizer," *Opt. Lett*., vol. 21, pp. 336-338, 1996.

[4] P. F. Wysocki, J. B. Judkins, R. P. Espindola, M. Andrejco, and A. M. Vengsarkar, "Broad-band erbium-doped fiber amplifier flattened beyond 40 nm using long-period grating filter," *IEEE Photon. Technol. Lett*., vol. 9, pp. 1343-1345, 1997.

[5] M. K. Pandit, K. S. Chiang, Z. H. Chen, and S. P. Li, "Tunable long-period fiber gratings for EDFA gain and ASE equalization," *Microwave and Opt. Technol. Lett*., vol. 25, pp. 181-184, 2000.

[6] D. B. Stegall and T. Erdogan, "Dispersion control with use of long-period fiber gratings," *J. Opt. Soc. Am. A*, vol. 17, pp. 304-312, 2000.

[7] V. Bhatia, D. Campbell, R. O. Claus, and A. M. Vengsarkar, "Simultaneous strain and temperature measurement with long-period gratings," *Opt. Lett*., vol. 22, pp. 648-650, 1997.

[8] H. J. Patrick, C. C. Chang, and S. T. Vohra, "Long period fibre gratings for structural bend sensing," *Electron. Lett*., vol. 34, pp. 1773-1775, 1998.

[9] V. Grubsky and J. Feinberg, "Long-period fiber gratings with variable coupling for real-time sensing applications," *Opt. Lett*., vol. 25, pp. 203-205, 2000.

[10] M. N. Ng, Z. Chen, and K. S. Chiang, "Temperature compensation of long-period fiber grating for refractive-index sensing with bending effect," *IEEE Photon. Technol. Lett*., vol. 14, pp. 361-363, 2002.

[11] K. S. Chiang, Y. Liu, M. N. Ng, and S. Li, "Coupling between two parallel long-period fibre gratings," *Electron. Lett.*, vol. 36, pp. 1408-1409, 2000.

[12] K. S. Chiang, M. N. Ng, Y. Liu, and S. Li, "Evanescent-field coupling between two parallel long-period fiber gratings," in *Proc. IEEE Lasers and Electro-Optics Society Conf.*, Puerto Rico, 2000, pp. 836-837.

[13] V. Grubsky, D. S. Starodubov, and J. Feinberg, "Wavelength-selective coupler and add-drop multiplexer using long-period fiber gratings," in *Tech. Dig., Optical Fiber Communication Conf.*, 2000, vol. 4, pp. 28-30.

[14] K. S. Chiang, F. Y. M. Chan, and M. N. Ng, "Analysis of two parallel long-period fiber gratings," *J. Lightwave Technol.*, vol. 22, pp. 1358-1366, 2004.

[15] V. Rastogi and K. S. Chiang, "Long-period gratings in planar optical waveguides," *Appl. Opt.*, vol. 41, pp. 6351-6355, 2002.

[16] Q. Liu, K. S. Chiang, and V. Rastogi, "Analysis of corrugated long-period waveguide gratings and their polarization dependence," *J. Lightwave Technol.*, vol. 21, pp. 3399-3405, 2003.

[17] K. S. Chiang, K. P. Lor, C. K. Chow, H. P. Chan, V. Rastogi, and Y. M. Chu, "Widely tunable long-period gratings fabricated in polymer-clad ion-exchanged glass waveguides," *IEEE Photon. Technol. Lett.*, vol. 15, pp. 1094-1096, 2003.

[18] K. S. Chiang, C. K. Chow, H. P. Chan, Q. Liu, and K. P. Lor, "Widely tunable polymer long-period waveguide grating with polarization-insensitive resonance wavelength," *Electron. Lett.*, vol. 40, pp. 422-424, 2004.

[19] Y. M. Chu, Q. Liu, and K. S. Chiang, "Control of temperature sensitivity of long-period waveguide grating by etching of cladding," in *Proc. 9th Optoelectronics and Communications Conf. (OECC 2004)*, Yokohama, Japan, 2004, pp. 920-921.

[20] M.-S. Kwon and S.-Y. Shin, “Characteristics of polymer waveguide notch filters using thermooptic long-period gratings,” *IEEE J. Selected Topics Quantum Electron.*, vol 11, pp. 190-196, 2005.

[21] M.-S. Kwon and S.-Y. Shin, “Polymer waveguide notch filter using two stacked thermooptic long-period gratings,” *IEEE Photonics Technol. Lett.*, vol. 17, pp. 792-794, 2005.

[22] K. P. Lor, Q. Liu, and K. S. Chiang, “UV-written long-period gratings on polymer waveguides,” *IEEE Photon. Technol. Lett.*, vol. 17, pp. 594-596, 2005.

[23] G. Griffel, M. Itzkovich, and A. A. Hardy, “Coupled mode formulation for directional couplers with longitudinal perturbation,” *IEEE J. Quantum Electron.*, vol. 27, pp. 985-994, 1991.

[24] W. P. Huang, B. E. Little, and S. K. Chaudhuri, “A new approach to grating-assisted couplers,” *J. Lightwave Technol.*, vol. 9, pp. 721-727, 1991.

[25] A. S. Sudbo, “Numerically stable formulation of the transverse resonance method for vector mode-field calculations in dielectric waveguides,” *IEEE Photon. Technol. Lett.*, vol. 5, pp. 342-344, 1993.

[26] M. Svalgaard, “Ultraviolet light induced refractive index structures in germanosilica,” Ph.D. thesis, (Mikroelektronik Centret, Technical University of Denmark, Lyngby, Denmark), pp. 88-94, 1997.

[27] M. R. Poulsen, P. I. Borel, J. Fage-Pedersen, J. Hűbner, M. Kristensen, J. H. Povlsen, K. Rottwitt, M. Svalgaard, and W. Svendsen, “Advances in silica-based integrated optics,” *Opt. Eng.*, vol. 42, pp. 2821-2834, 2003.

Figure Captions:

Fig. 1 Schematic diagram of a waveguide coupler consisting of two parallel identical cores, each of which contains a corrugated long-period grating.

Fig. 2 (a) Transmission spectra and (b) coupling dynamics at λ_0 for an LPWG coupler consisting of two perfectly aligned LPWGs with $C = 0$ and $\kappa L = \pi/\sqrt{2}$.

Fig. 3 (a) Transmission spectra and coupling dynamics at (b) $\delta = 0$ and (c) $\delta L = 8\pi$ for an LPWG coupler consisting of two perfectly aligned LPWGs with $C = 0$ and $\kappa L = 3\pi/\sqrt{2}$.

Fig. 4 (a) Transmission spectra and coupling dynamics at (b) $\delta = 0$ and (c) $\delta L = 24\pi$ for an LPWG coupler consisting of two perfectly aligned LPWGs with $C = 0$ and $\kappa L = 5\pi/\sqrt{2}$.

Fig. 5 Dependence of the normalized 3-dB bandwidth of the rejection band of an LPWG coupler on the value of *n*.

Fig. 6 (a) Transmission spectra and (b) coupling dynamics at λ_0 for an LPWG coupler consisting of two perfectly aligned LPWGs with $CL = 4\pi/3$ and $\kappa L = \pi/3\sqrt{5/2}$.

Fig. 7 Transmission spectra for an LPWG coupler consisting of two perfectly aligned LPWGs with $\kappa L = \pi/\sqrt{2}$ and (a) CL = 0, 0.01, and 0.1; (b) CL = 0.3 and 1.

Fig. 8 (a) Transmission spectra and (b) coupling dynamics at λ_0 for an LPWG coupler consisting of two partially offset LPWGs with $z_1 = \pi/2\kappa$ and $z_2 - z_1 = \pi/\sqrt{2}\kappa$.

Fig. 9 (a) Transmission spectra and (b) coupling dynamics at λ_0 for an LPWG coupler consisting of two completely offset LPWGs with $z_1 = L = \pi/2\kappa$.

Fig. 10 Dependence of the effective indices of the even (E_{11}) and odd (E_{21}) guided modes of the entire structure for both quasi-TE and quasi-TM polarizations on the core separation d of the waveguide structure in Fig. 1 with n_{core} = 1.537, n_{clad} = 1.505, n_{sub} = 1.444, n_{ex} = 1, a = h = 3 μm, s = 6 μm, and t = 4 μm.

Fig. 11 (a) Phase matching curves for couplings to different cladding modes and (b) dependence of the effective indices of different modes on the wavelength for an LPWG coupler with n_{core} = 1.537, n_{clad} = 1.505, n_{sub} = 1.444, n_{ex} = 1, a = h = 3 μm, s = 6 μm, t = 4 μm, and d = 8 μm.

Fig. 12 Dependence of the coupling coefficient κ for couplings to the quasi-TE and quasi-TM E_{31} and E_{41} modes on the grating corrugation depth Δh for an LPWG coupler with waveguide parameters as for Fig. 11.

Fig. 13 Transmission spectra for coupling to the E_{31} cladding mode of an LPWG coupler with a grating pitch of 93.2 μm and other parameters as for Fig. 11: (a) the quasi-TE polarization; (b) the quasi-TM polarization.

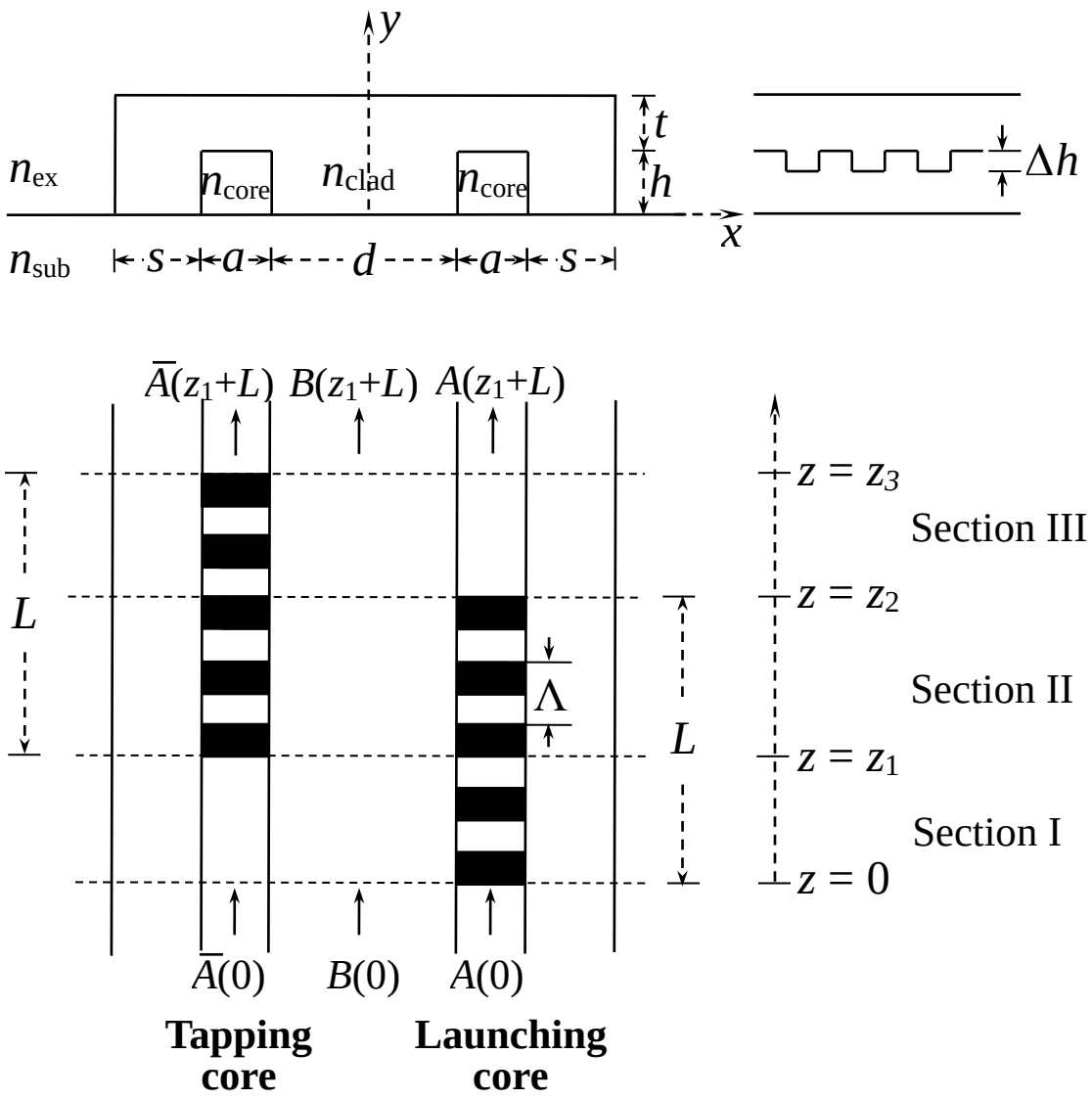
y
t
h
Δh
n_ex
n_core
n_clad
n_core
x
n_sub
s
a
d
a
s
Ā(z1+L)
B(z1+L)
A(z1+L)
z = z3
Section III
z = z2
Section II
z = z1
Section I
z = 0
L
Λ
L
Ā(0)
B(0)
A(0)
Tapping core
Launching core

Fig. 1

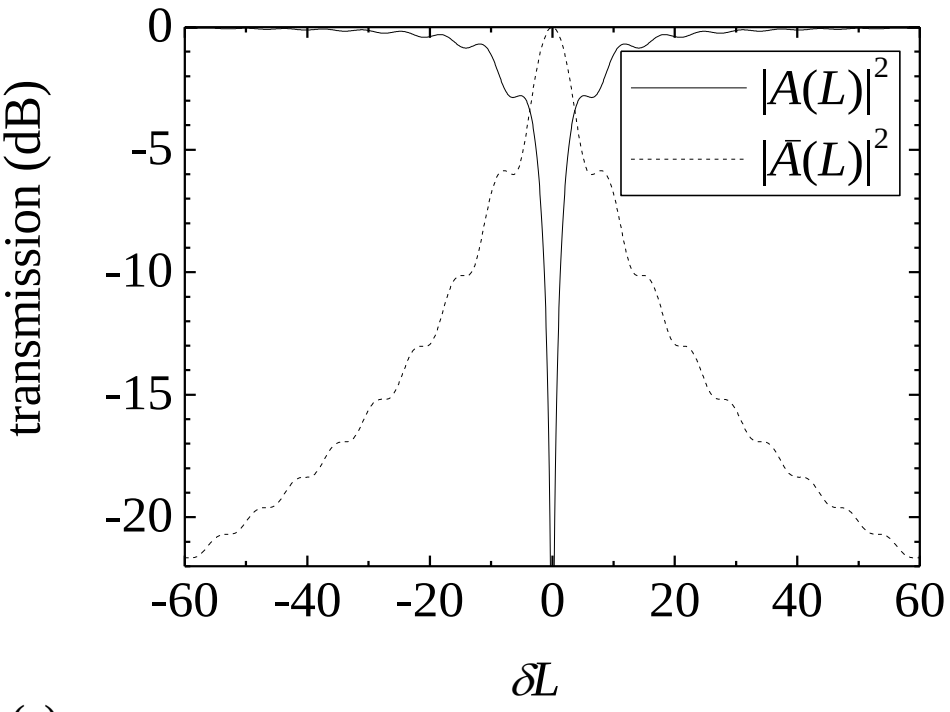
transmission (dB)
0
-5
-10
-15
-20
-60
-40
-20
0
20
40
60
δL
$|A(L)|^2$
$|\bar{A}(L)|^2$

(a)

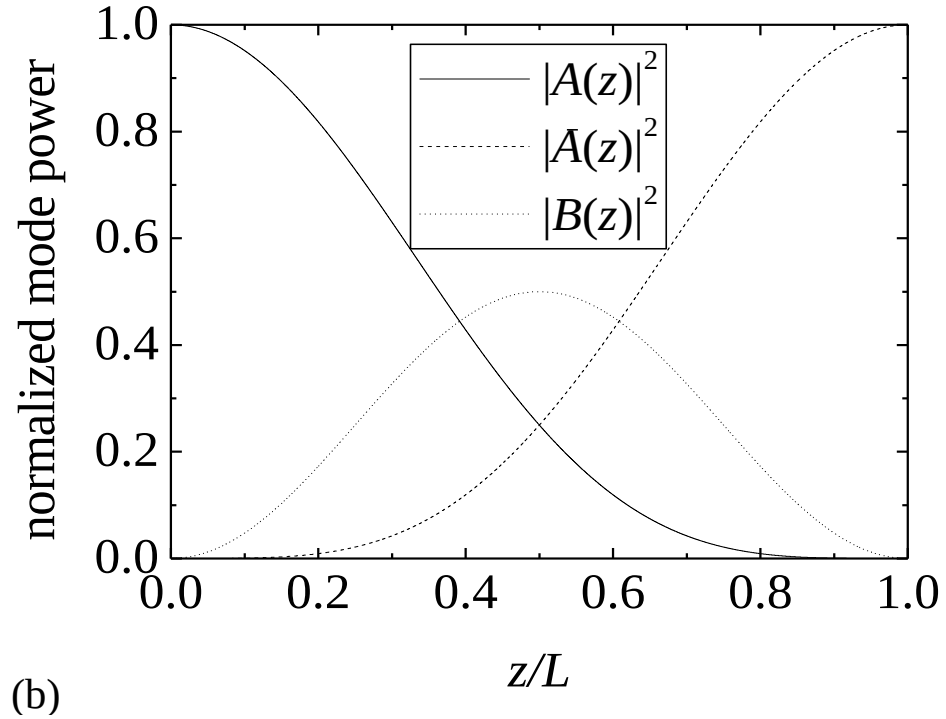
normalized mode power
1.0
0.8
0.6
0.4
0.2
0.0
0.0
0.2
0.4
0.6
0.8
1.0
z/L
$|A(z)|^2$
$|\bar{A}(z)|^2$
$|B(z)|^2$

(b)

Fig. 2

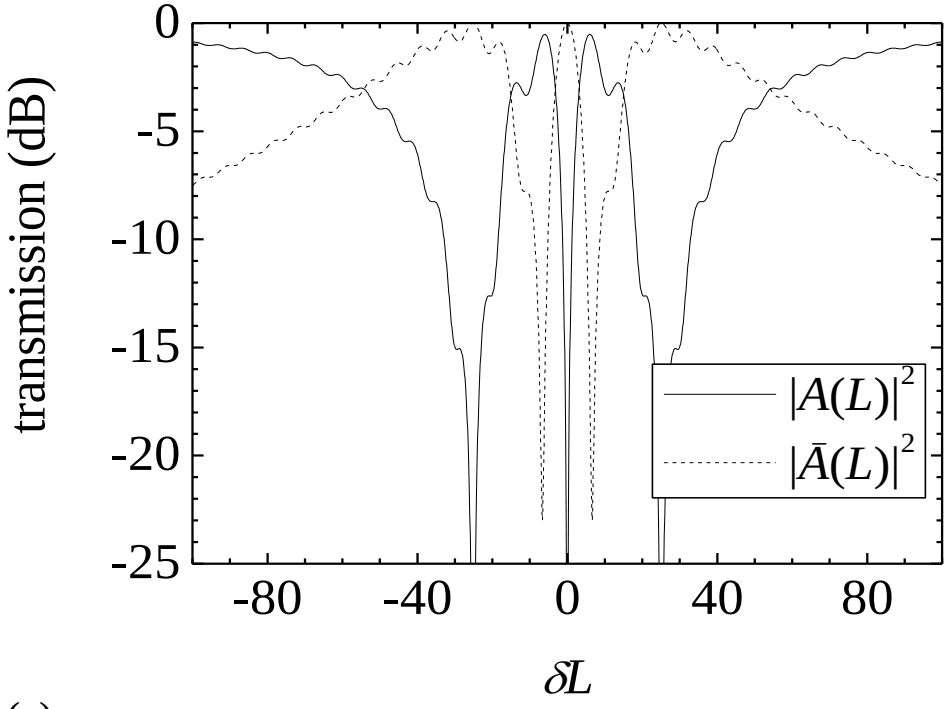
transmission (dB)
0
-5
-10
-15
-20
-25
-80
-40
0
40
80
δL
|A(L)|²
|Ā(L)|²

(a)

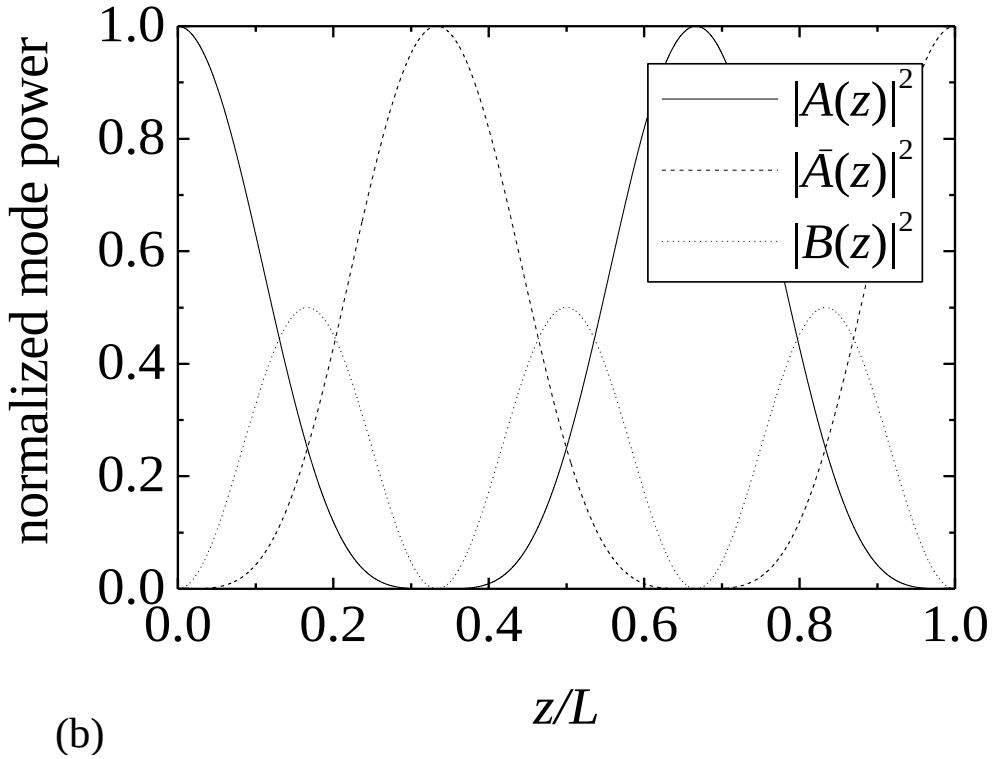
normalized mode power
1.0
0.8
0.6
0.4
0.2
0.0
0.0
0.2
0.4
0.6
0.8
1.0
z/L
|A(z)|²
|Ā(z)|²
|B(z)|²

(b)

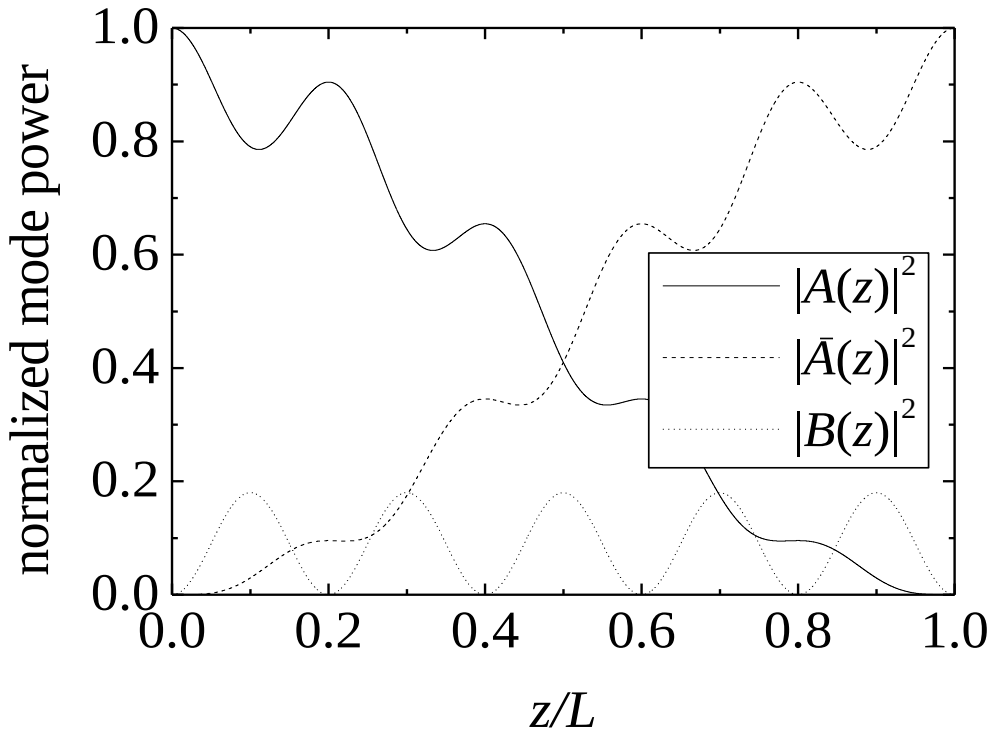
normalized mode power
1.0
0.8
0.6
0.4
0.2
0.0
0.0
0.2
0.4
0.6
0.8
1.0
z/L
$|A(z)|^2$
$|\bar{A}(z)|^2$
$|B(z)|^2$

(c)

Fig. 3

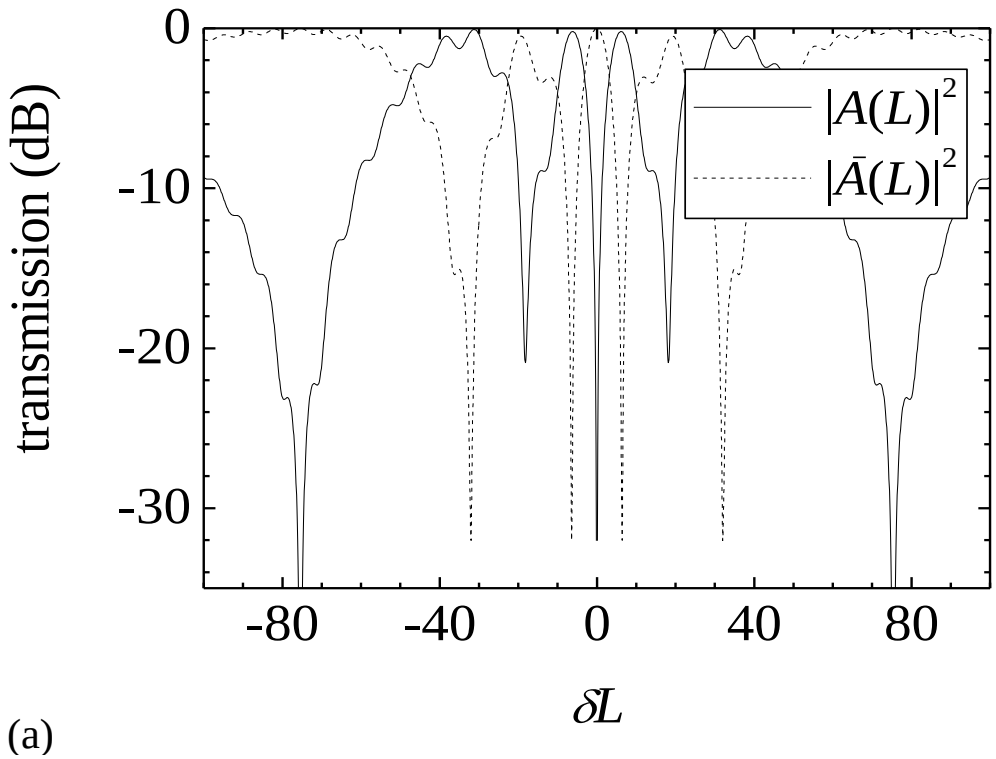
transmission (dB)
0
-10
-20
-30
-80
-40
0
40
80
δL
$|A(L)|^2$
$|\bar{A}(L)|^2$

(a)

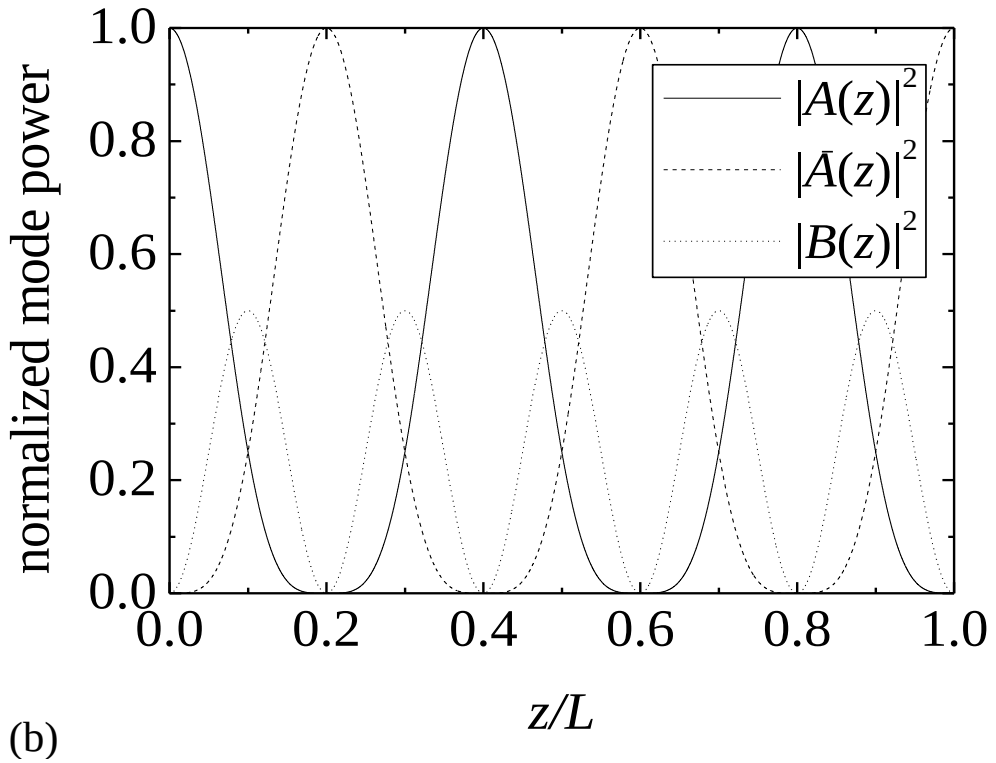
normalized mode power
1.0
0.8
0.6
0.4
0.2
0.0
0.0
0.2
0.4
0.6
0.8
1.0
z/L
$|A(z)|^2$
$|\bar{A}(z)|^2$
$|B(z)|^2$

(b)

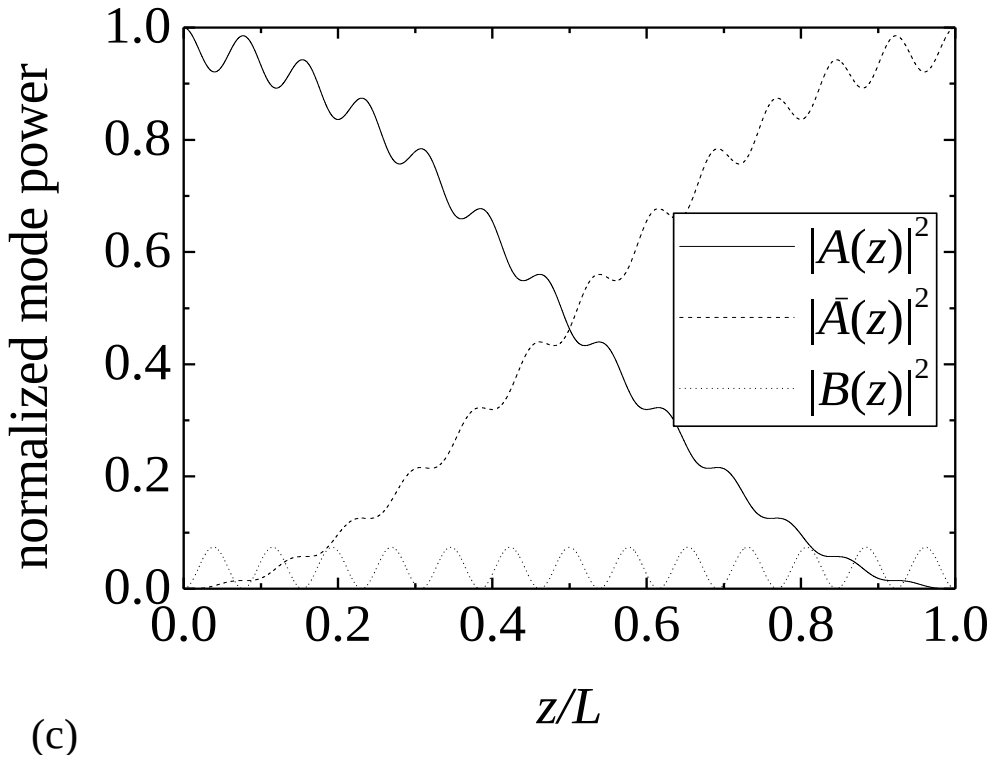
normalized mode power
1.0
0.8
0.6
0.4
0.2
0.0
0.0
0.2
0.4
0.6
0.8
1.0
z/L
|A(z)|^2
|Ā(z)|^2
|B(z)|^2

(c)

Fig. 4

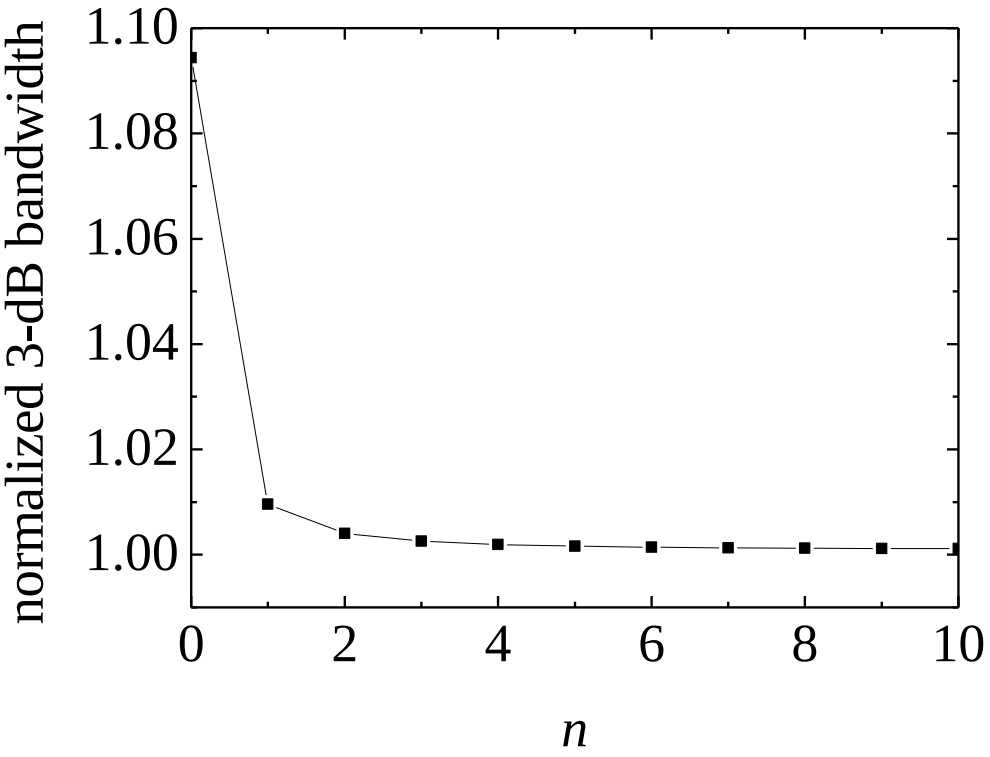

Fig. 5

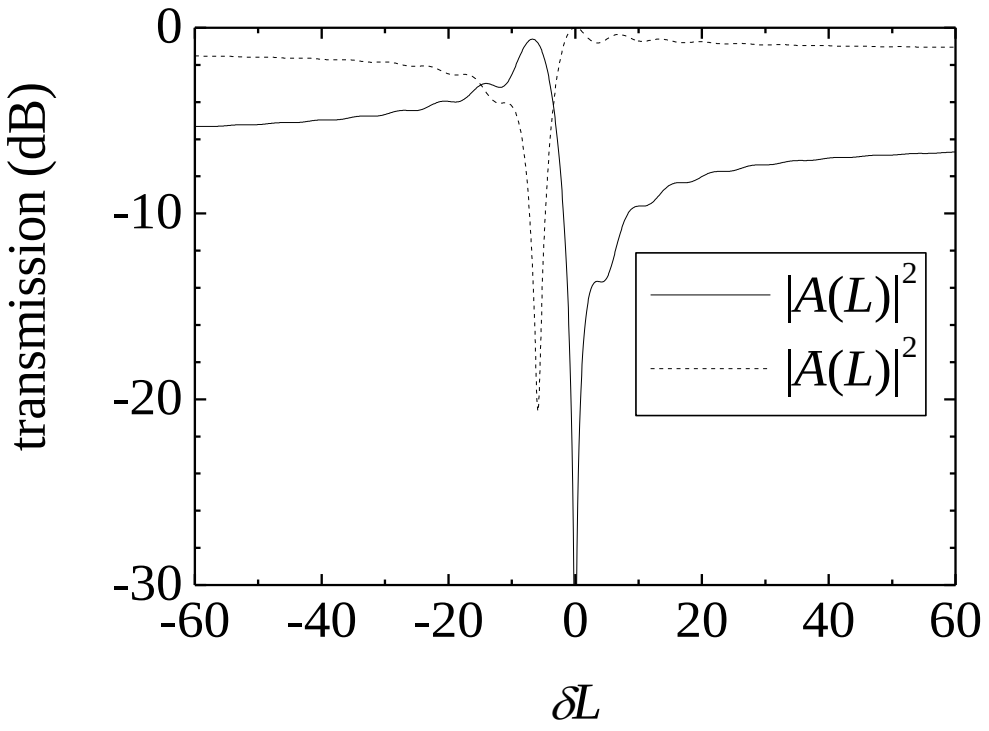
transmission (dB)
0
-10
-20
-30
-60
-40
-20
0
20
40
60
δL
$|A(L)|^2$
$|A(L)|^2$

(a)

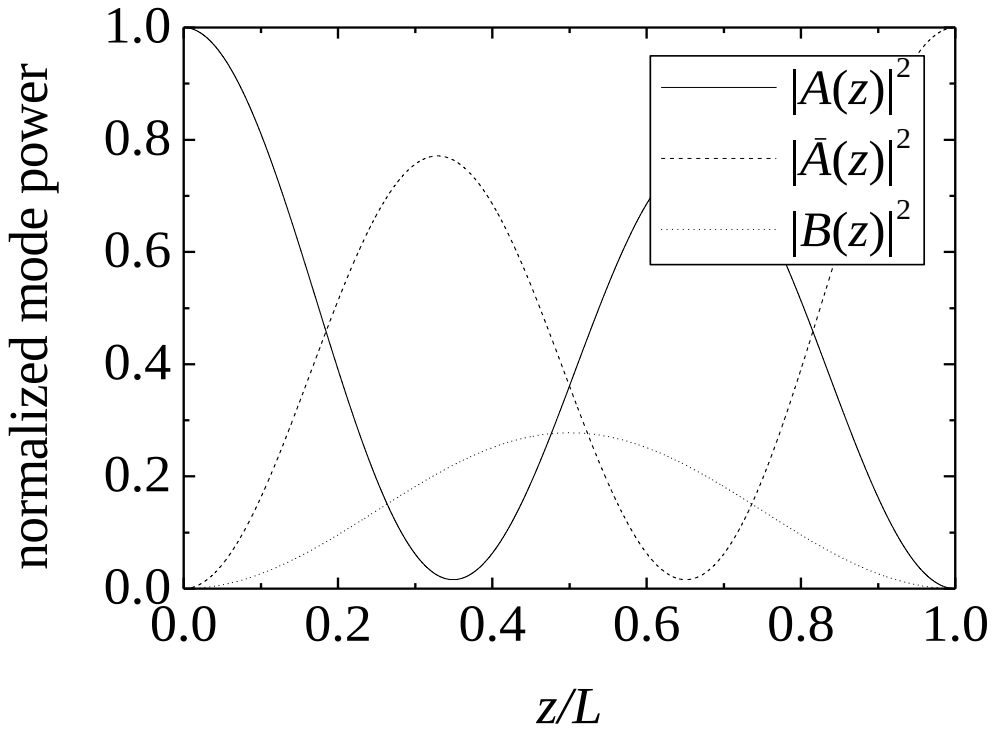
normalized mode power
1.0
0.8
0.6
0.4
0.2
0.0
0.0
0.2
0.4
0.6
0.8
1.0
z/L
$|A(z)|^2$
$|\bar{A}(z)|^2$
$|B(z)|^2$

(b)

Fig. 6

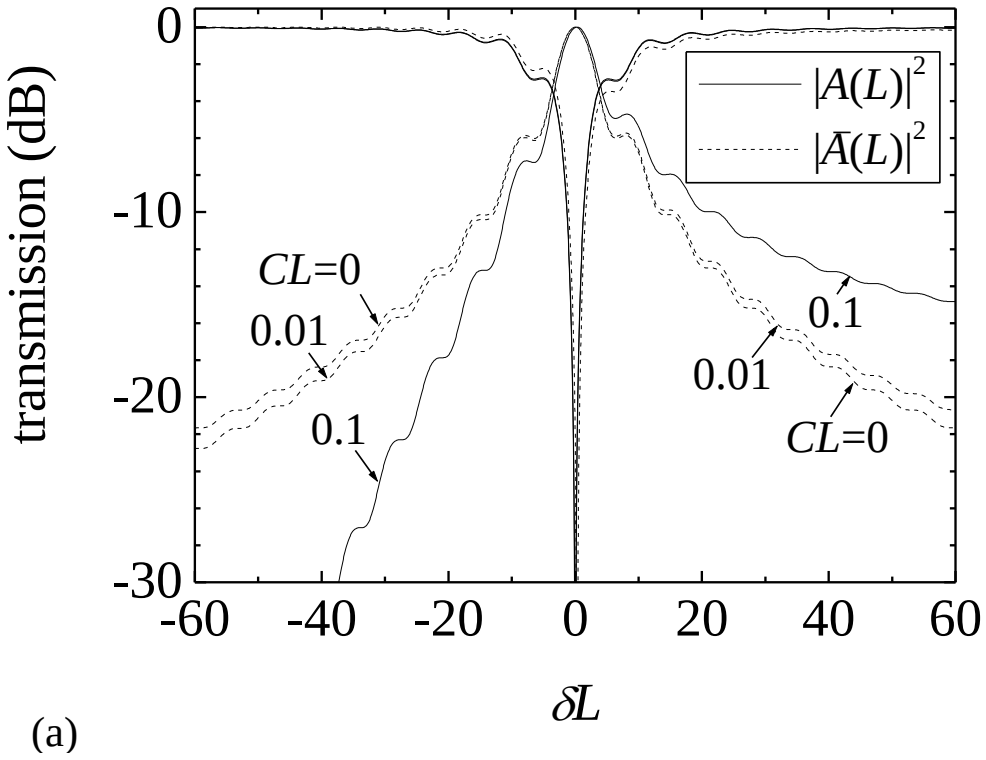
transmission (dB)
0
-10
-20
-30
-60
-40
-20
0
20
40
60
δL
$|A(L)|^2$
$|\bar{A}(L)|^2$
CL=0
0.01
0.1
0.1
0.01
CL=0

(a)

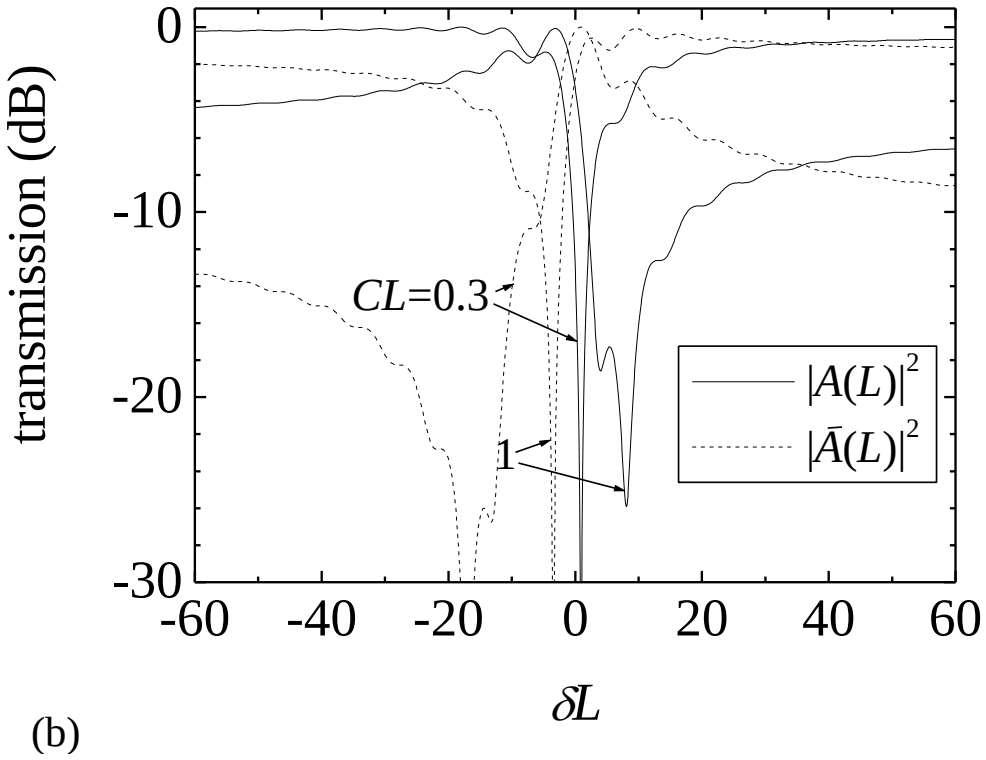
transmission (dB)
0
-10
-20
-30
-60
-40
-20
0
20
40
60
δL
CL=0.3
1
$|A(L)|^2$
$|\bar{A}(L)|^2$

(b)

Fig. 7

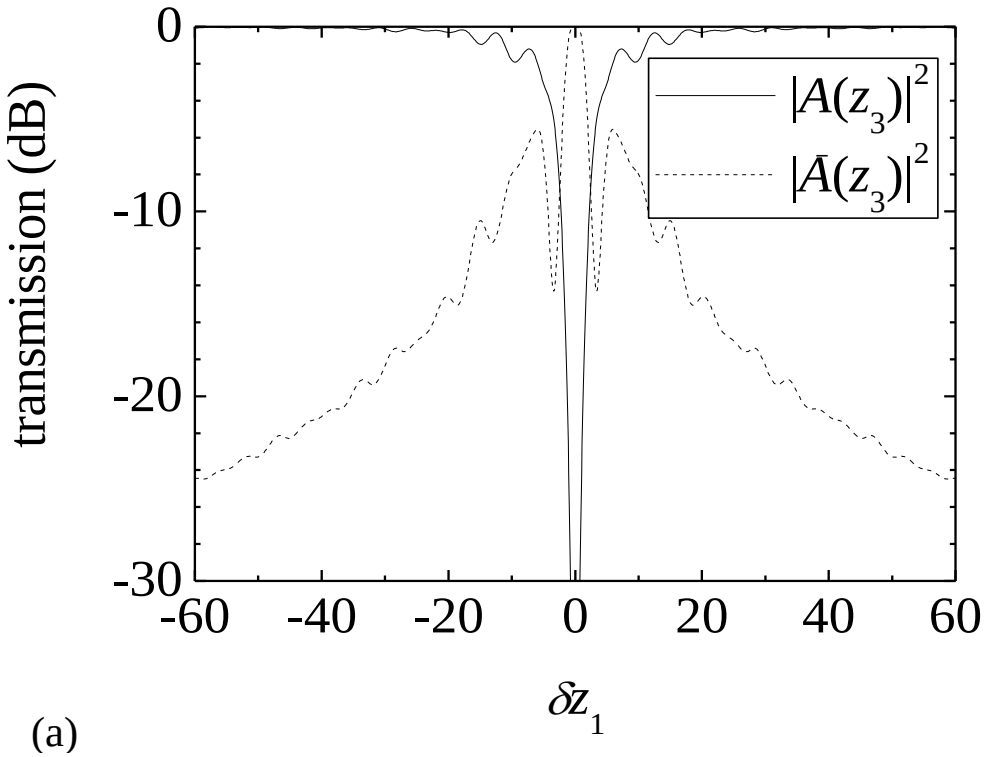
transmission (dB)
0
-10
-20
-30
-60
-40
-20
0
20
40
60
$|A(z_3)|^2$
$|\bar{A}(z_3)|^2$
δz_1

(a)

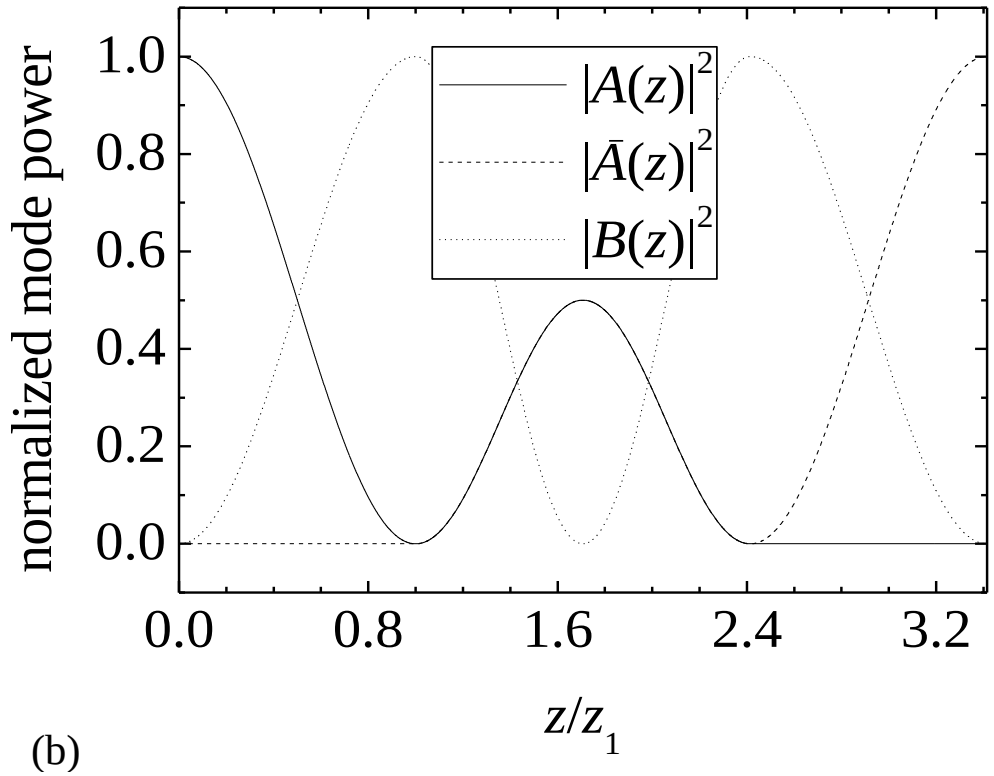
normalized mode power
1.0
0.8
0.6
0.4
0.2
0.0
0.0
0.8
1.6
2.4
3.2
$|A(z)|^2$
$|\bar{A}(z)|^2$
$|B(z)|^2$
z/z_1

(b)

Fig. 8

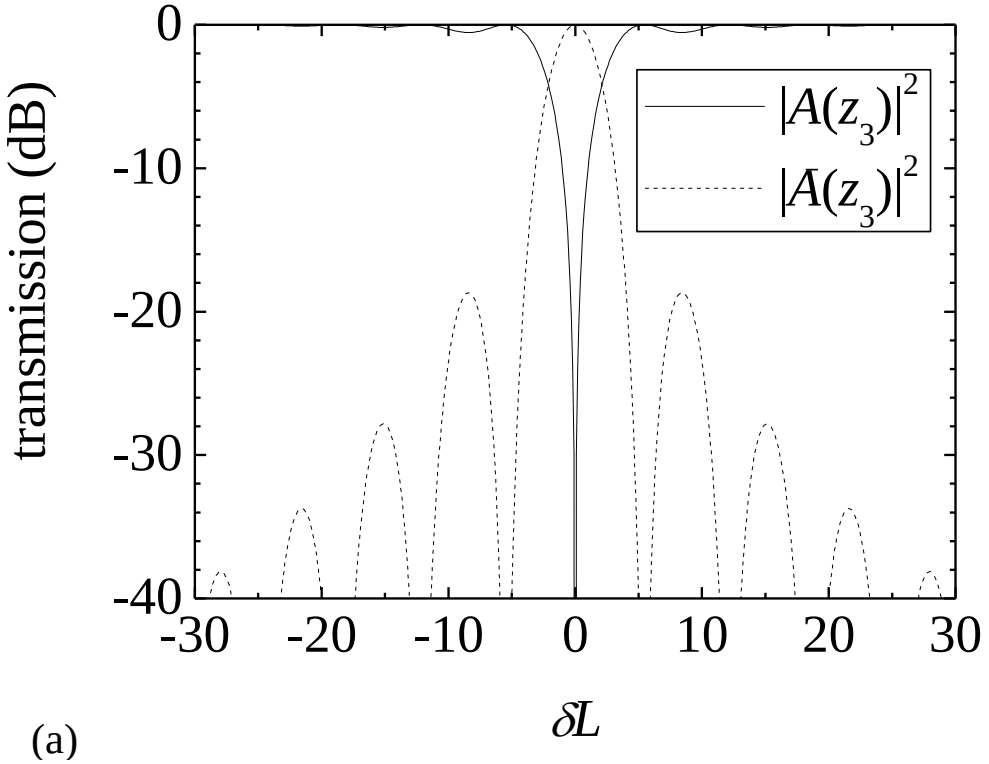
transmission (dB)
0
-10
-20
-30
-40
-30
-20
-10
0
10
20
30
δL
$|A(z_3)|^2$
$|\bar{A}(z_3)|^2$

(a)

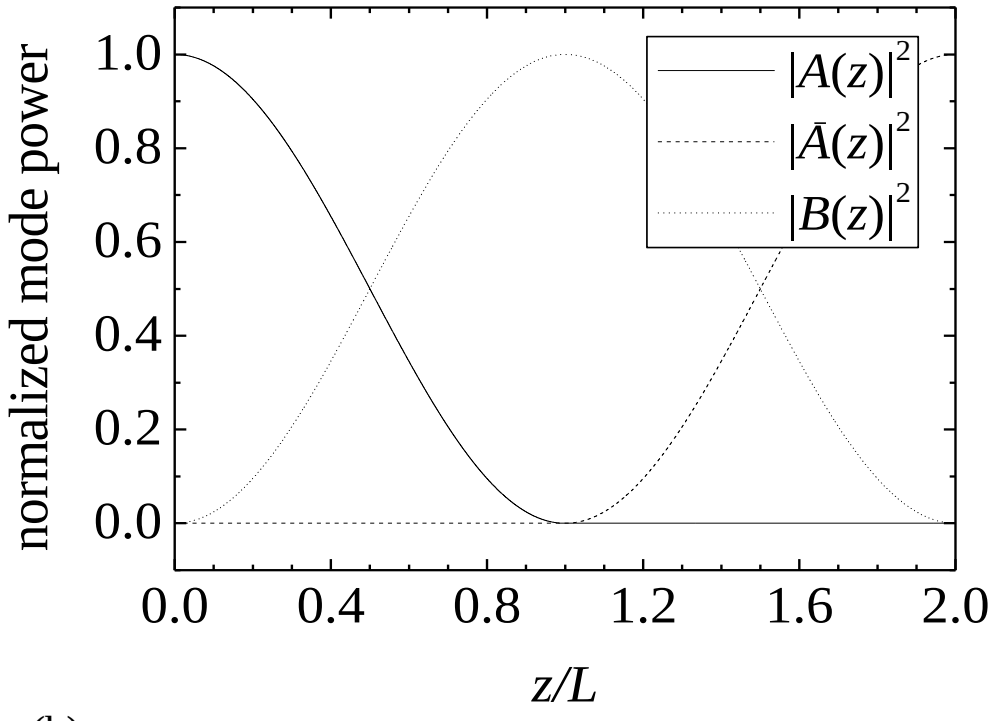
normalized mode power
1.0
0.8
0.6
0.4
0.2
0.0
0.0
0.4
0.8
1.2
1.6
2.0
z/L
$|A(z)|^2$
$|\bar{A}(z)|^2$
$|B(z)|^2$

(b)

Fig. 9

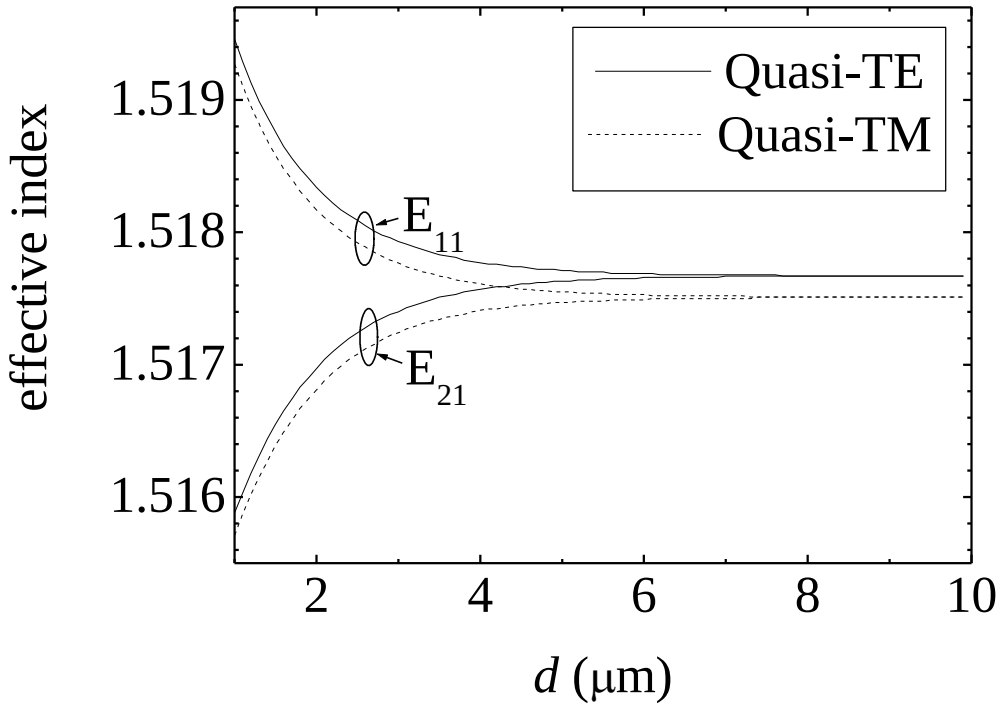
effective index
1.519
1.518
1.517
1.516
2
4
6
8
10
d (μm)
Quasi-TE
Quasi-TM
E11
E21

Fig. 10

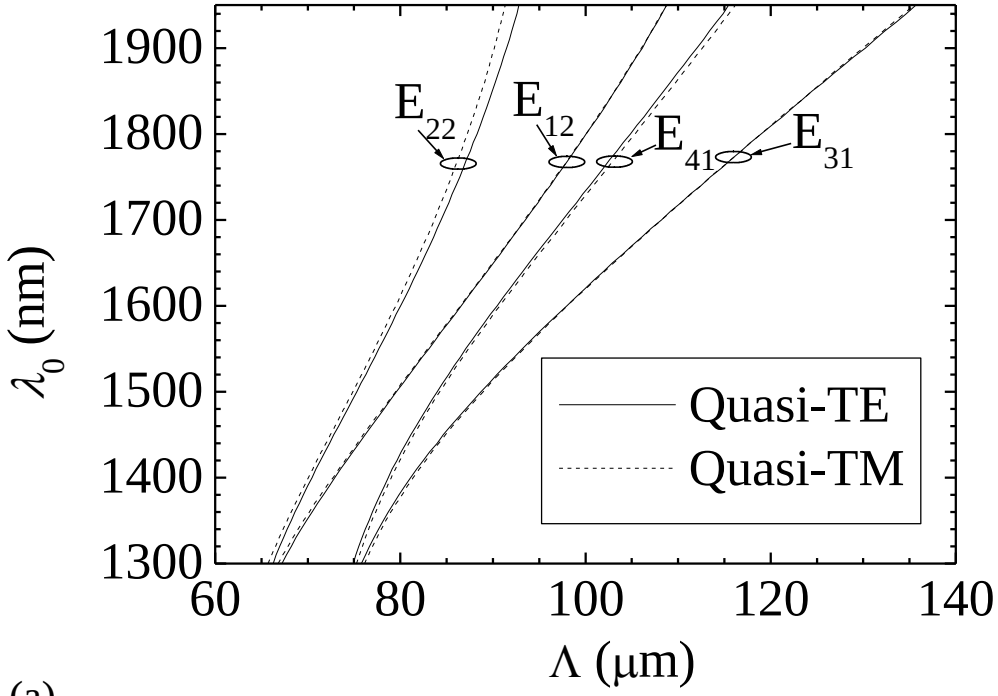
1900
1800
1700
1600
1500
1400
1300
60
80
100
120
140
λ0 (nm)
Λ (μm)
E22
E12
E41
E31
Quasi-TE
Quasi-TM

(a)

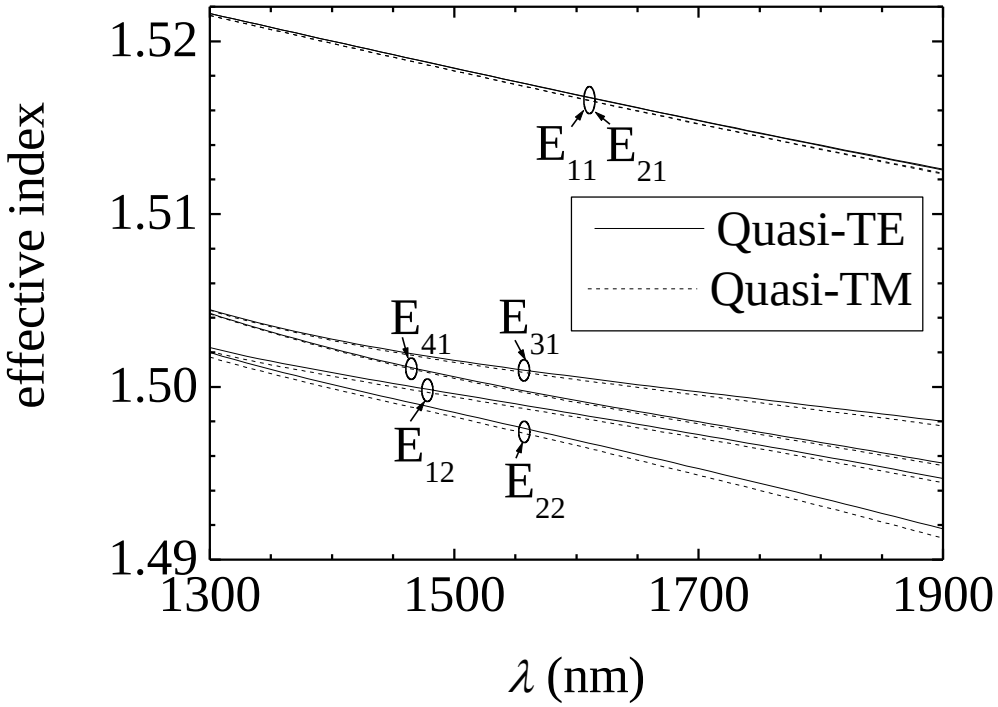
1.52
1.51
1.50
1.49
1300
1500
1700
1900
effective index
λ (nm)
E11
E21
E41
E31
E12
E22
Quasi-TE
Quasi-TM

(b)

Fig. 11

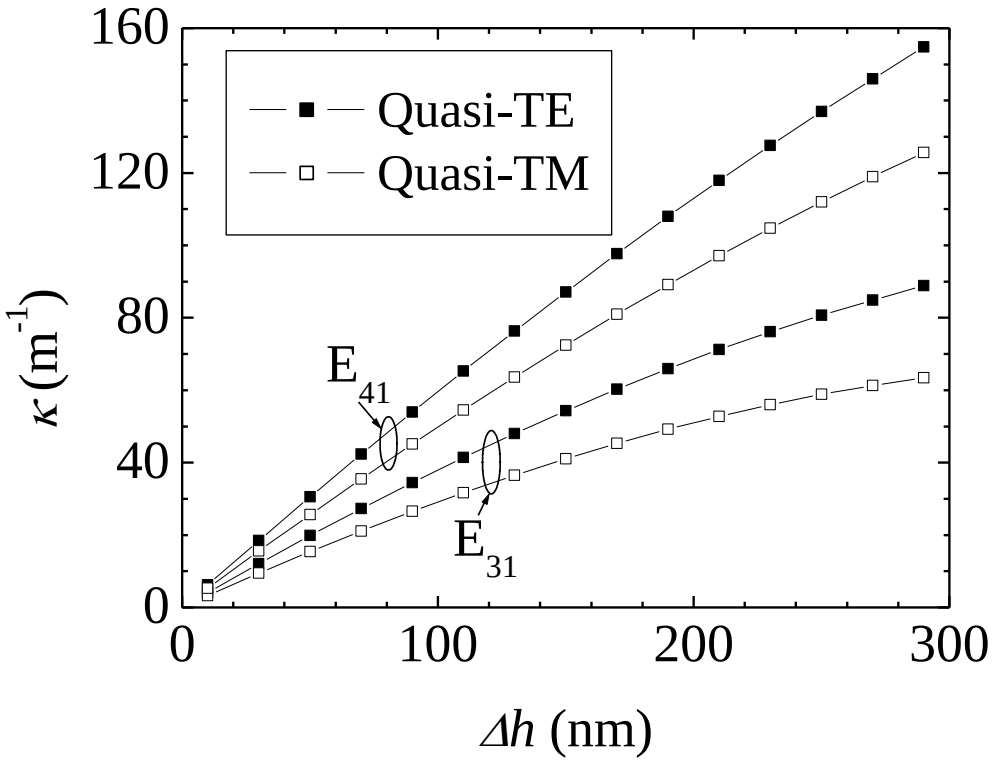

Fig. 12

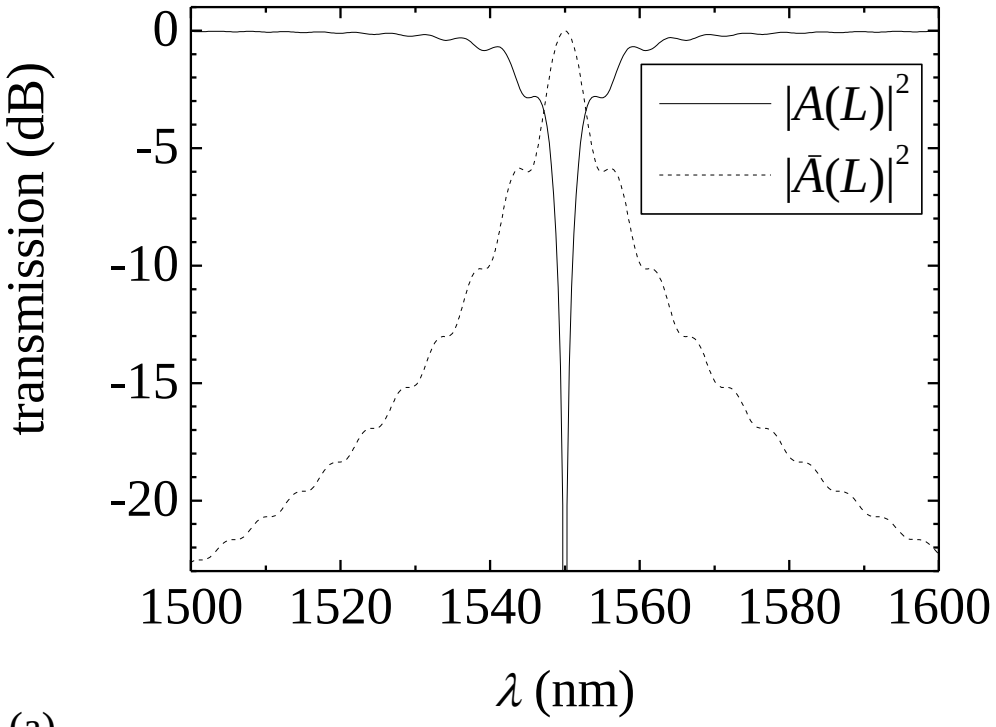
transmission (dB)
0
-5
-10
-15
-20
1500
1520
1540
1560
1580
1600
λ (nm)
$|A(L)|^2$
$|\bar{A}(L)|^2$

(a)

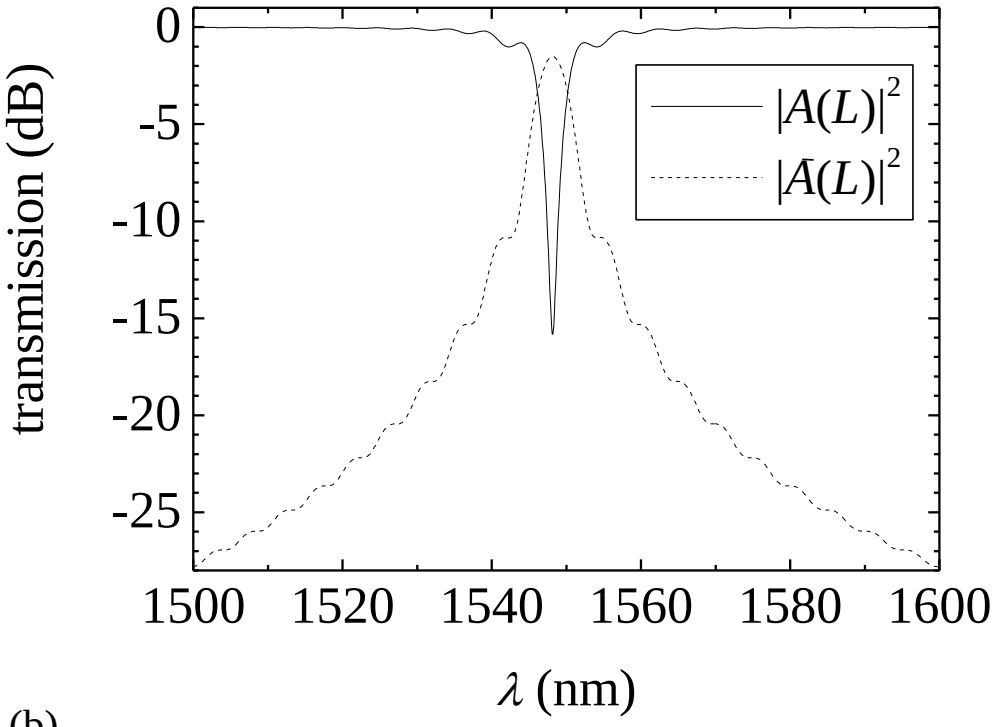
transmission (dB)
0
-5
-10
-15
-20
-25
1500
1520
1540
1560
1580
1600
λ (nm)
$|A(L)|^2$
$|\bar{A}(L)|^2$

(b)

Fig. 13